Insights into Digit Evolution from a Fate Map Study of the Forearm

Oh, JDH[1], Saunders, DDZ[1], McTeir, L[1], Jackson, M[2], Glover, JD[2] Schoenebeck, JJ[2], Lettice, LA[3], Davey, MG[1].

[1]Functional Genetics, The Roslin Institute R(D)SVS, CMVM, University of Edinburgh, UK EH25 9RG

[2]Genetics and Genomics, The Roslin Institute R(D)SVS, CMVM, University of Edinburgh, UK EH25 9RG

[3]MRC Human Genetics Unit, Institute of Genetics and Cancer, University of Edinburgh, Edinburgh, UK EH4 2XU

Abstract

The cellular and genetic networks which contribute to the development of the zeugopod, (radius and ulna of the forearm, tibia and fibula of the leg) are not well understood, although these bones are susceptible to loss in congenital human syndromes and to the action of teratogens such as thalidomide. Using a new fate mapping approach in transgenic chickens, we show that there is a small contribution of *SHH* expressing cells to the posterior ulna, posterior carpals and digit 3. We establish that while the majority of the ulna develops in response to paracrine SHH signaling in both the chicken and mouse, there are differences in the contribution of *SHH* expressing cells to other tissues of the zeugopod between these two species as well as between the chicken ulna and fibula. This is evidence that although zeugopod bones are clearly homologous according to the fossil record, the zeugopod bones of the wing and leg are formed by subtly different signalling and patterning events during embryonic development, which can be used to understand the shaping of the bird wing skeleton during the evolution of powered flight.

Introduction

Limbs first form as small paired forelimb or hindlimb buds growing from the flank of a developing embryo (Tickle, 2015). The mesodermal cell component of the limb bud, derived from the lateral plate mesoderm (Gros and Tabin, 2014), forms the majority of the limb skeleton from the proximal shoulder/pelvic girdle to the digit tips. The cells that make up the early limb look homogenous but fate maps of the early chicken wing bud show that at stage 20HH (Hamburger and Hamilton, 1951), mesodermal-derived cells within specific areas are already fated to form either the shoulder/pelvic girdle, stylopod (humerus/femur) or zeugopod (radius and ulna, tibia/fibula), and by HH24, the autopod (digits; Dudley et al., 2002; Nomura et al., 2014; Sato et al., 2007; Saunders, 1948; Vargesson et al., 1997). Within the autopod, the origin, number and signalling pathways which pattern the antero-posterior identity of digits have been well studied (Harfe et al., 2004; Tamura et al., 2011; Towers et al., 2008; Towers et al., 2011; Zhu et al., 2022). Although the specification of the zeugopod region within the proximo-distal axis of limb bud has been examined (Dudley et al., 2002; McCusker and Rosello-Diez, 2022; Rosello-Diez et al., 2011; Sato et al., 2007) how two bones with different antero-posterior identities, the anterior radius and posterior ulna, develop from this area has not been thoroughly investigated. Human conditions highlight the separate identities of these bones in that there are notable differences between conditions where either the radius or ulna is lost. Radial deficiency is more common than ulnar deficiency, even in thalidomide cases where it is more common to observe the loss of entire proximo-distal segments. Unlike radial deficiency, ulnar deficiency is rarely associated with systemic syndromes (Bednar et al., 2009).

The zeugopod is, however, subject to many of the same patterning mechanisms as the autopod and parallels between these parts of the limb can be drawn, specifically between the antero-posterior axis patterning by SHH and FGF pathways (Chiang et al., 2001; Mariani et al., 2008). A loss of FGF signaling in the mouse or inhibition of cell proliferation in the chicken limb bud causes a loss of anterior digits and the radius, evidence that these tissues are dependent on cell proliferation driven by FGF signaling (Mariani et al., 2008; Towers et al., 2008; Towers and Tickle, 2009). In the chicken wing, *SHH* is expressed in the mesoderm-derived organiser of the limb, the 'Zone of Polarising Activity' (ZPA), from stage 18HH and it is thought that the relative balance of paracrine and autocrine SHH signaling, along with cell proliferation, is central to establishing both digit number and identity (Towers et al., 2008; Zhu et al., 2022). In the human, mouse or chicken, a loss of SHH causes a loss of posterior digits and a loss of the ulna (Chiang et al., 2001; Ianakiev et al., 2001; Ros et al., 2003; Towers et al., 2008), demonstrating that SHH signaling is required for posterior limb identity in either the zeugopod or autopod and that the ulna is a SHH-dependent bone. In addition there is a distinction between the derivatives of cells expressing *SHH* within the ZPA organiser and subject to autocrine SHH signalling and those which are patterned by the ZPA organiser, receiving paracrine SHH signals. In the mouse, *Shh* expressing cells from the ZPA contribute to digits 3-5 as well as the ulna (Harfe et al., 2004; Scherz et al., 2007), indicating that a portion of the ulna is patterned by autocrine Shh signaling as well as paracrine signaling (Ahn and Joyner, 2004). The contribution of *SHH* expressing cells to the ulna has not been examined in the chick, although unlike the 5-fingered mouse, *SHH* expressing cells do not contribute to any of the three digits of the wing (Towers et al., 2011). This has been used as evidence to determine which two digits birds lost during evolution towards powered flight (Tamura et al., 2011; Towers et al., 2011; Xu and Mackem, 2013), an important paradigm in the study of evolutionary development (Evo-Devo).

The evolution of the bird wing, in particular understanding which two digits were 'lost' and which three remain in the modern tridactyly wing, is studied both to understand the context of the bird wing as a model of vertebrate limb development and morphological evolution (Brusatte, 2017; Richardson et al., 2009). The focus on the majority of the research in this area has been to understand which of the three bird digits are homologous to a five of a pentadactyl limb, such as a mouse, human or basal archosaur, an example of which is the basal tetrapod *Westlothiana* (Smithson et al., 2011) from which all limbs' pattern arose. There are conflicting interpretations of digit homology due to an incomplete fossil record and confounded by an ambiguity in assigning a universal digit identity to either the three bird digits, using either adult or embryological data (Burke and Feduccia, 1997; Chatterjee, 1998; de Bakker et al., 2013; de Bakker et al., 2021; Hinchliffe and Hecht, 1984; Kawahata et al., 2019; Larsson and Wagner, 2002; Richardson, 2012; Salinas-Saavedra et al., 2014; Stewart et al., 2019; Tamura et al., 2011; Towers, 2018; Towers et al., 2008; Towers et al., 2011; Vargas and Fallon, 2005; Welten et al., 2005; Woltering and Duboule, 2010; Xu and Mackem, 2013; Xu et al., 2014). In these studies, evolutionary anatomical changes in the zeugopod bones, have been overlooked as homology of the radius and ulna is easily assigned and both are clearly present throughout the fossil record. Rather, the emphasis has been that morphology of the carpals and digits has evolved distal to the 'unchanging' bony anatomy of the forearm, the radius and ulna (Fig. 1D). This is embodied in the a foundation principal, the 'primary limb axis' hypothesis (Salinas-Saavedra et al., 2014; Shubin and Alberch, 1986), which emphasises the line of conserved morphology that includes the humerus and ulna around which distally digits have evolved. How palaeontological, anatomical and embryological data have been interpreted has led to the development of the 'frame-shift' and 'axis-shift' hypotheses (Xu and Mackem, 2013).

98

99 The ‘frame-shift’ model (Fig. 1E), primarily based on embryological evidence such as the
100 development of *SOX9*+ digit primordia, proposes that the primary axis is maintained and the
101 ulna-digit 4 articulation remains unchanged, but that a modified digit 4 takes on a
102 morphological identity of a digit III through a homeotic transformation, thereby concluding
103 that digit 1 and 5 are lost (de Bakker et al., 2013). Alternatively based on both fossil and
104 embryological data, specifically the contribution of *SHH* expressing cells to the digits as a
105 indicator of lineage, the ‘axis-shift’ model (Fig. 1F) suggests that the articulation between the
106 primary axis/ulna shifts from digit 4 to digit 3, but does not account for how the change in
107 this relationship might have occurred (Towers et al., 2011). A limitation of all these studies
108 has been a lack of analysis of the bones proximal to the digits although analysis of the carpals
109 suggests that these bones, articulating the zeugopod with the autopod, have been even more
110 radically altered than the digits (Botelho et al., 2014). We propose that understanding
111 developmental events which pattern the limb proximal to the digits, including the
112 contribution of *SHH* expressing cells to elements of the posterior bird forelimb and carpals, is
113 central to understanding the evolution of the avian primary limb axis and digits that articulate
114 with it. We therefore sought to identify the exact location of the ulna anlage and explore its
115 relation to the ZPA using a new anatomical approach to fate mapping in the developing
116 chicken embryo. We show that, like the mouse, SHH ZPA cells contribute to the chicken
117 ulna, carpals and digit 3 cartilage in a developmental stage dependent manner, demonstrating
118 an embryological relationship between these skeletal elements.

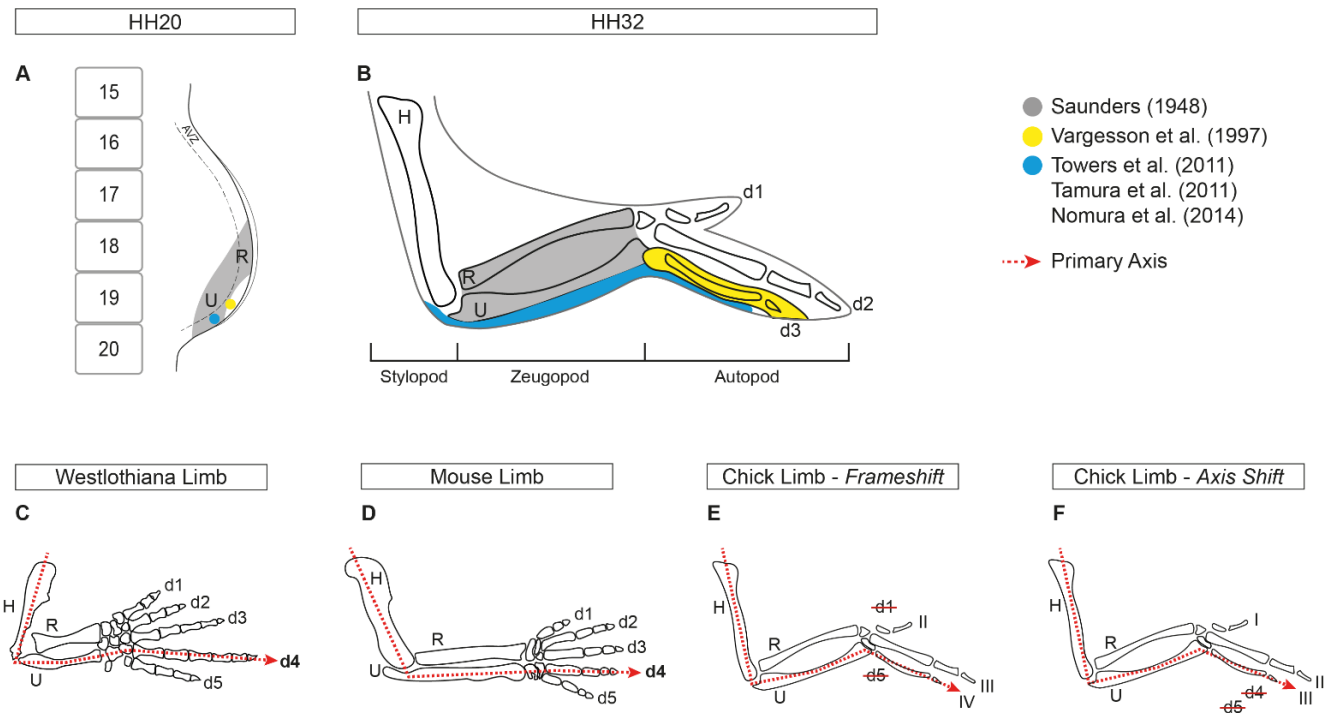

Figure 1. Summary of published fate maps and hypotheses for digit loss in chicken.

Amalgamation of previous fate map studies of the chick wing with (**A**) showing the stage 20HH chick wing bud with somites and avascular zone as reference and (**B**) showing the stage 32HH chick wing. Grey shading derived from Saunders (1948) and yellow shading from Vargesson et al. (1997). Blue shading show an agreement of results from Towers et al. (2011), Tamura et al. (2011) and Nomura et al. (2014). Diagram of the primary axis represented by a red dotted line going through the humerus, ulna and digit 4 in (**C**) the Westlothiana limb and (**D**) mouse limb. (**E**) Schematic of the frameshift hypothesis, in which the primary axis continues to course through the ulna and digit 4 in the chick wing, with a loss of digits 1 and 5. (**F**) Schematic of the axis shift hypothesis, in which the primary axis has shifted and now courses through digit 3 in the chick wing.

<u>Abbreviations</u> HH: Hamburger Hamilton. AVZ: Avascular zone. H: Humerus. R: Radius. U: Ulna. d: digit.

Results

The ulna arises from a discrete area within the chick limb bud

To locate the area from which the ulna is specified in the stage 20HH chick wing bud, we employed a novel fate map technique that utilises the Chameleon cytbow chicken line in conjunction with TAT-Cre recombinase (Davey et al., 2018). Initially, all cells in the Chameleon chick embryo ubiquitously express nuclear H2B-eBFP2. Addition of beads soaked with TAT-Cre recombinase to the Chameleon chick embryo induces recombination at the cytbow transgene, deleting the nuclear H2B-eBFP2 and allowing expression of one of the three fluorescent proteins: eYFP, tdTomato or mCFP (accompanying Bio-Protocol paper; Saunders et al.). The action of TAT-Cre protein in the developing embryo is both highly localised to the area of application and transient, lasting less than a minute, resulting in small discrete induction of stable fluorescence expression which can be subsequently assessed clonally.

As the ulna is known to be dependent on SHH signaling, we first examined the fate of the presumptive zeugopod forming region at 20HH as identified by Saunders (1948; Fig. 1A, B). With Saunders' map as a guide, beads soaked in TAT-Cre recombinase were inserted around the ulnar area of the presumptive zeugopod forming region in 20HH Chameleon chicken limb buds to determine that the ulna arises from cells in the distal limb bud, parallel to the anterior half of somite 19 (Fig. 2A, B). This region of the limb lies above the *SHH* expressing ZPA cells but expresses *PTCH1*, a hedgehog receptor whose expression is induced by the ligand, demonstrating the area is subject to paracrine SHH signaling (Fig. 2C, C''). Stage 33HH wings were subsequently analysed for anatomical distribution of fluorescent cells, which were found to be located in the ulna, posterior carpals and digit 3 (n=3; Fig. 2D-J). Beads placed either more proximally or within the ZPA parallel to the posterior half of somite 19,

158 which expresses both *SHH* and *PTCH1,* did not result in fluorescent labelling of the ulna
159 (n=5; Supplementary Fig. 1).

160 Closer analysis of limbs labelled at the anterior half somite 19 (*SHH-/PTCH1+*),
161 demonstrated that fluorescent cells spanned the length of the ulna (Fig. 2D-G) and were
162 largely contained within the ulna cartilage (Fig. 2E-G) indicating that cells within 50µm of
163 the bead at stage 20HH contributed to the entire length of the ulna. Sections showed no
164 labelled cells in the radius (Fig. 2F) and few cells in the ulnar perichondrium or adjacent soft
165 tissues (n=3/3, Fig. 2E-G). In addition to the ulna, the cartilage of posterior carpals (Fig. 2H)
166 and the cartilage of digit 3 (Fig. 2J) also contained fluorescent cells, as well as soft tissue
167 adjacent to the cartilage of digit 2 (Fig. 2I; n=3/3).

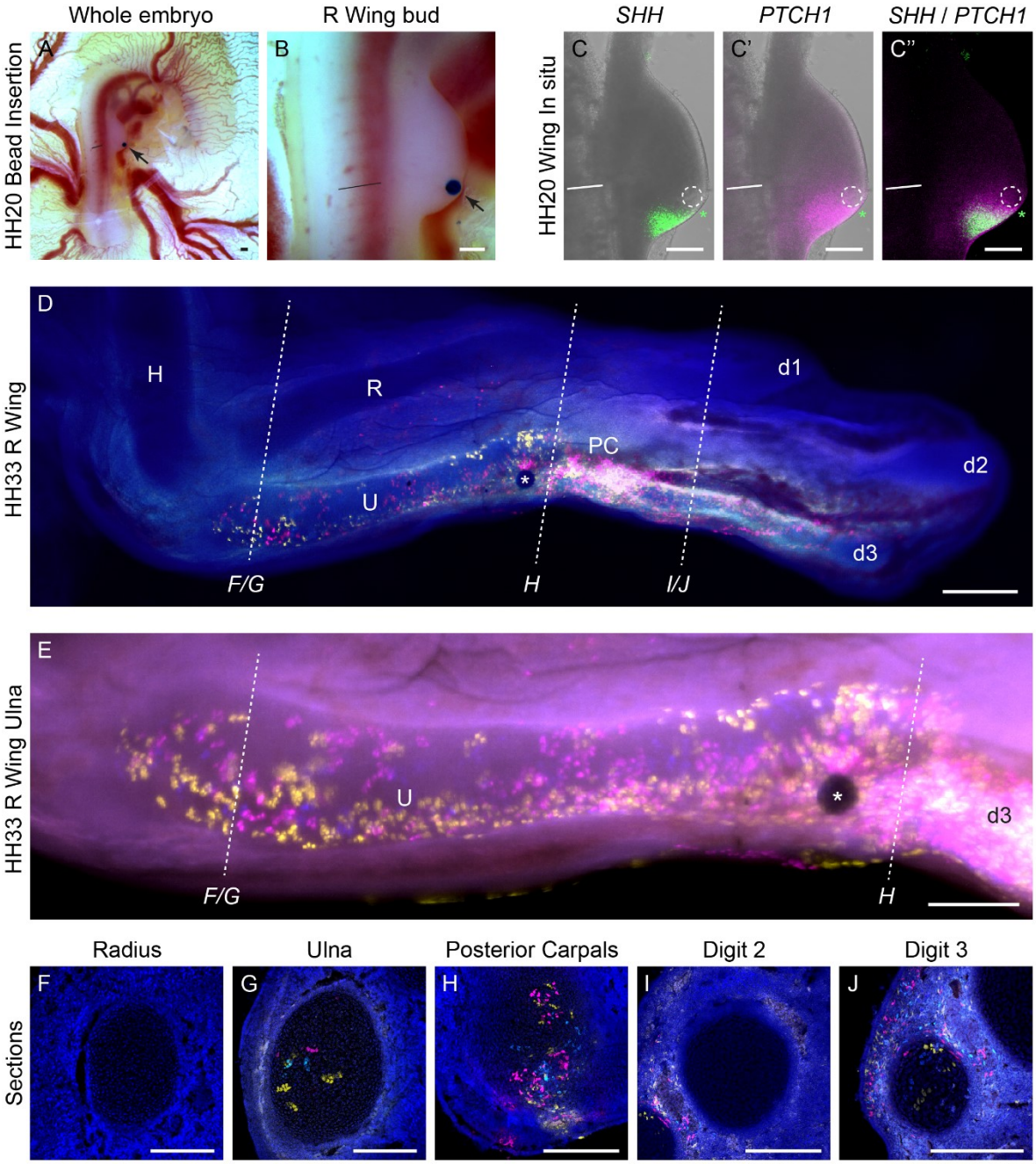

Figure 2. Fate map of chick ulna using Chameleon chickens.

Placement of beads soaked in TAT-Cre (arrow) that maps the ulna in stage 20HH Chameleon chick wing buds shown in (**A**) whole embryo and (**B**) and at higher magnification. Stage 20HH chick wing buds with inert bead (dashed white circle) inserted in anterior half of somite 19, same as (**B**) then HCR in situ hybridisation performed with (**C**) *SHH* and (**C'**) *PTCH1* both shown against brightfield. Merge of *SHH* and *PTCH1* shown in (**C''**). Asterisk

denotes the anterior-most edge of the ZPA. Straight black and white lines denote the anterior-most edge of somite 19.

Chameleon stage 33HH chick wing showing fluorescent cells (magenta, yellow and cyan with white indicating overlap) in the ulna and digit 3 (**D**) which were recombined on exposure to TAT-Cre delivered by bead as per (**B**). Close-up of the same limb with focus on ulna (**E**). Dashed lines in (**D**) and (**E**) denote where sections of the radius (**F**), ulna (**G**), posterior carpals (**H**), digit 2 (**I**) and digit 3 (**J**) were taken. White asterisk denotes location of bead.

Abbreviations HH: Hamburger Hamilton. AVZ: Avascular zone. H: Humerus. R: Radius. U: Ulna. PC: Posterior carpals. d1/2/3: digit 1/2/3.

All scale bars = 200μm

186 ***SHH* expressing cells make a small contribution to the ulna in a stage-dependent**
187 **manner**

188 Our fate mapping approach, like others before, creates small and discrete clones of labelled
189 cells. While excellent for generating fate maps with high spatial resolution, it does not
190 demonstrate the fate of all the cells in a specific region. For example, no single bead
191 application labelled all the cells of an ulna (Fig. 2D). Until recently it has been generally
192 presumed that each bone forms from one area, or primordia, which can be sufficiently
193 represented by small clones of labelled cell in fate napping approaches. Using a different fate
194 mapping approach in mouse, it has recently been shown that rather than expanding over time
195 and differentiating in a proximal to distal order from one primordia, limb bones, including the
196 ulna, form piecemeal with different parts of the bone differentiating at different times but
197 eventually forming one entity (Markman et al., 2023), although this evidence is not
198 inconsistent with individual bones arising from one primordia. To assess if the area we had
199 identified was able to generate all the cells of the ulna, we undertook homotopic grafting of
200 the presumptive ulna primordia between stage 20/21HH eGFP and dtTomato transgenic
201 chicken embryos. Distal wing mesenchyme grafts from dtTomato stage 20HH limbs,
202 corresponding to the anterior of somite 19 and approximately 150µm by 150µm in size (Fig.
203 3A), were grafted into the equivalent area in eGFP embryos (Fig. 3B). To confirm that grafts
204 were correctly taken from the *SHH*-/*PTCH1*+ domain we observed examined gene expression
205 in donor limbs after grafts were excised, via HCR RNA in situ hybridisation and confirmed
206 that all grafts originated from the *SHH*-/*PTCH1*+ presumptive ulna primordia (Fig. 3M-
207 M'''). qRT-PCR was used to assess expression in mock grafts from the presumptive ulna
208 primordia which were also found to be *SHH*-/*PTCH1*+ (Fig. 3L). tdTom grafts of the
209 presumptive ulna primordia gave rise to the cartilage of the ulna and carpals (n=7/7; Fig. 3C-
210 D') and digit 3 (n=5/7) in host eGFP embryos. Unlike labelling of the ulna primordia via

211 TAT-Cre application, contribution to the entire length of the ulna was dependent on graft size
212 as smaller grafts only gave rise to the distal ulna, carpals and digit (n=4/7). However, this
213 demonstrates that the cells which generate the ulna at stage 20/21HH come from within the
214 distal *SHH*-/*PTCH1*+ domain, outside of the *SHH* expressing ZPA.

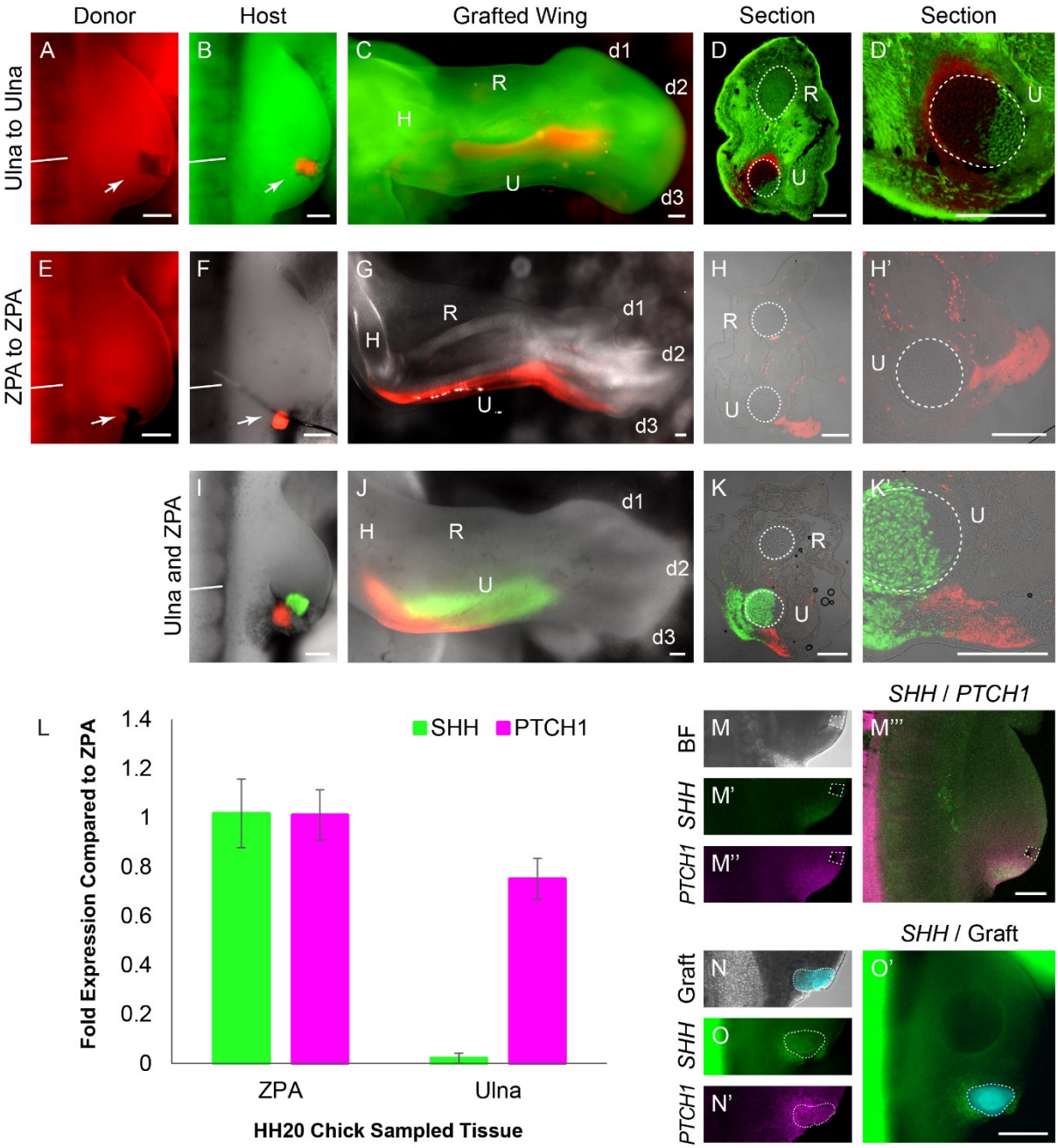

215

216 **Figure 3. ZPA lineage in chick wing in association with *SHH* and *PTCH1* expressions**

217 Confirmation of Chameleon results by homotopic grafting of presumed ulna from stage
218 20HH tdTom chick wing bud (**A**) to eGFP chick wing bud (**B**). tdTom cells contribute to the
219 entire length of the ulna as shown in (**C**) with sections (**D**, **D'**) confirming tdTom cells in
220 cartilage. ZPA lineage determined through homotopic grafting of ZPA from stage 20HH
221 tdTom chick wing bud (**E**) to wild-type chick wing bud (**F**). tdTom cells do not contribute to

222 the ulna as shown in wholemount (**G**), confirmed with sections (**H**, **H'**). White arrows
223 indicate graft donor and host site. Homotopic double grafts with ZPA derived from a tdTom
224 chick wing bud and presumed ulna from an eGFP chick wing bud grafted into wild-type wing
225 bud (**I**). Subsequent wholemount (**J**) and sections (**K**, **K'**) show only eGFP cells contribute to
226 ulna. Dashed white circles outline the ulna and radius in sections. qRT-PCR for *SHH* (green)
227 and *PTCH1* (magenta) performed for 20HH ZPA, ulna and radius primordia (**L**). Close-up of
228 20HH chick wing with either presumed ulna excised (dashed white box) (**M**) then HCR in
229 situ hybridisation performed with *SHH* (**M'**) and *PTCH1* (**M''**). The same limb with merge
230 of *SHH* and *PTCH1* (**M'''**). Close-up of 20HH chick wing with eGFP ZPA grafted into wild-
231 type host (dashed white line) (**N**) then HCR in situ hybridisation performed with *SHH* (**O**)
232 and *PTCH1* (**N'**) with merge of *SHH* and graft in (**O'**). (**N**, **N'**) and (**O**, **O'**) are of the same
233 limb but imaged with confocal and fluorescent zoom microscopes, respectively. Straight
234 white lines denote the anterior-most edge of somite 19. Abbreviations H: Humerus. R:
235 Radius. U: Ulna. d1/2/3: digit 1/2/3. BF: Brightfield. All scale bars = 200µm.

236 It had previously been reported that in mice, the ulna arises from *SHH* expressing cells (Harfe
237 et al., 2004). In 20/21HH homochronic *SHH-*/*PTCH1+* domain grafts, complete ulna
238 labelling was observed in 3/7 samples. To confirm that stage 20/21HH chick ZPA cells
239 (*SHH+*/*PTCH1+*) do not contribute to the ulna, we performed homotopic ZPA grafts from
240 20HH dtTom or eGFP embryos (Fig. 3E) to either eGFP or non-transgenic chick wings (Fig.
241 3F). RT-qPCR was used to confirm expression of *SHH* and *PTCH1* in 'mock' ZPA grafts,
242 with around a 47 fold decrease in *SHH* of the ulna compared to the ZPA ($p<0.05$, Fig. 3L).
243 HCR RNA in situ hybridisation was used to assess expression of *SHH* and *PTCH1* in host
244 embryos containing grafts, confirming that grafted tissue originating from the ZPA
245 (*SHH+*/*PTCH1+*) was grafted into the ZPA region (*SHH+*/*PTCH1+*) in mock grafting
246 experiments (n=4, Fig. N-O'). All ZPA-ZPA stage 20HH grafts (n=3) contributed to the
247 posterior mesenchyme of the limb at stage 33HH but not the ulna, confirming that the stage
248 20HH ZPA does not contribute cells to the ulna (Fig. 3G-H').

249 To explore the interaction between ZPA cells and the ulnar primordium, both the ZPA
250 (tdTom) and the region giving rise to the ulna (eGFP) were transplanted together into
251 wildtype stage 20HH limb buds (Fig. 3I). At stage 33, there was no mixing of eGFP and
252 tdTomato cells in all limbs (Fig. 3J; n=3). Only eGFP cells (*SHH-*/*PTCH1+*) were within the
253 ulna cartilage and ZPA derived tdTom cells remained strictly outside of the cartilage (Fig.
254 3K, Supplementary Fig. 2).

255 These results demonstrate that the ulnar primordium is spatially defined, consistent with the
256 original chicken limb fate maps of Saunders (1948) and Summerbell (1974), but *SHH*
257 expressing cells do not contribute to the ulna in the chicken, as previously described in mouse
258 (Harfe et al., 2004).

259 To further explore potential differences in ulna specification between chicken and mouse we
260 re-examined the SHH reporter mouse SHH$^{tm1(EGFP/cre)Cjt}$ (Harfe et al., 2004; Scherz et al.,
261 2007). In combination with data from online resources (Baldarelli et al., 2021; J:184579; Shh
262 Embryo 3 E15.5; https://images.jax.org/webclient/img_detail/17489/) we confirm that, while
263 SHH expressing cells do contribute to the ulna and posterior mesenchyme of the zeugopod,
264 localisation is primarily in the distal ulna and is far less extensive than the contribution to
265 digit 4 and 5 (Harfe et al., 2004; Fig. 4A-E).

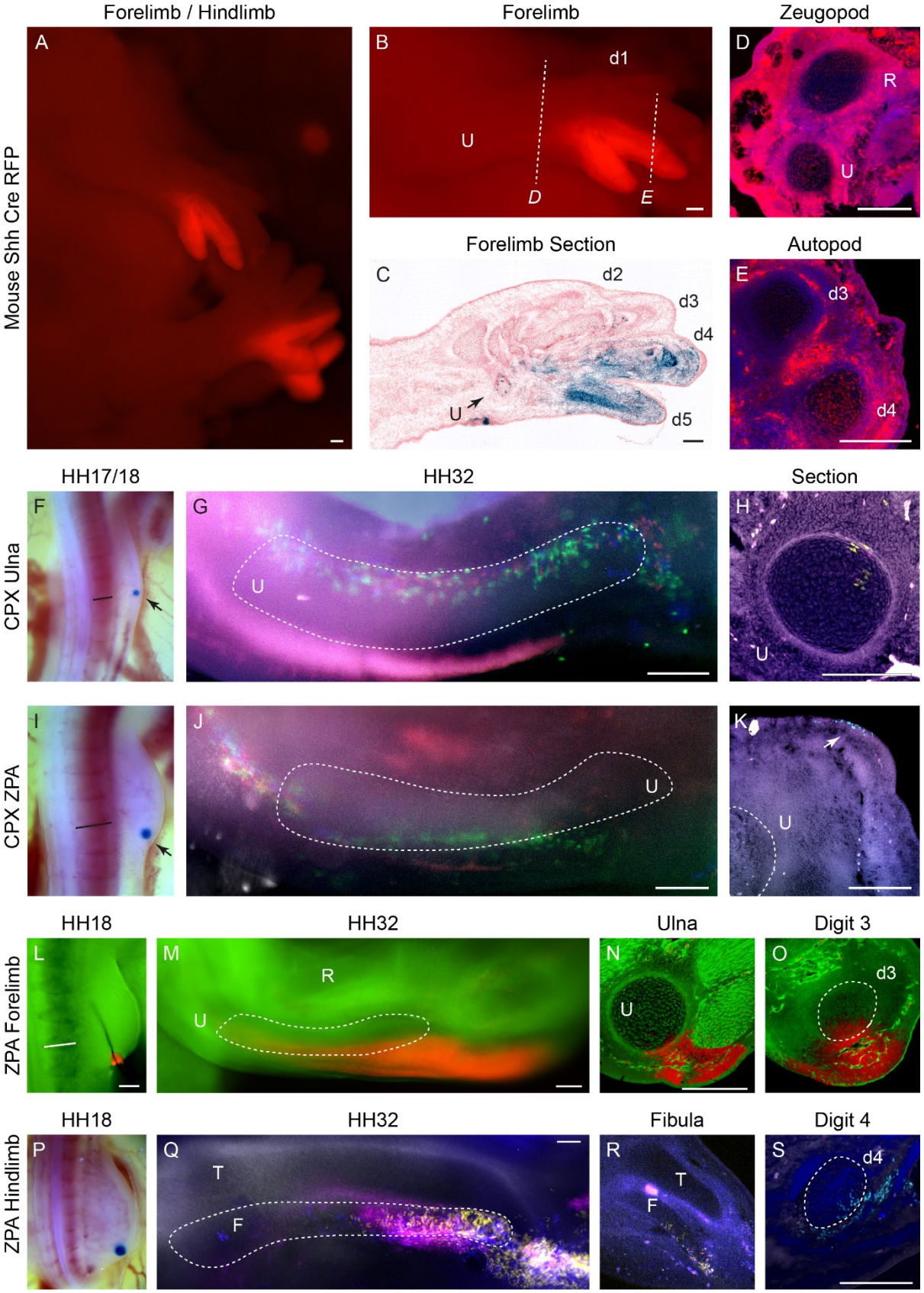

Figure 4. ZPA lineage in forelimbs and hindlimbs of mice and HH18 chicken.

268 **Figure 4. ZPA lineage in forelimbs and hindlimbs of mice and HH18 chicken.**

269 Right forelimb and hindlimb of an embryo carrying both $SHH^{tm1(EGFP/cre)Cjt}$ and a cre
270 inducible tdRFP reporter with RFP expression highlighting cells in the *SHH* lineage (**A**).
271 Same mouse with close-up of forelimb (**B**) with RFP in distal ulna and digits 4 and 5.
272 Longitudinal section from J:184579 (see main text) with blue showing *SHH* lineage (**C**).
273 Black arrow points to the distal ulna. Dashed lines in (**B**) denote where sections of the
274 zeugopod (**D**) and autopod (**E**) were taken with RFP in the cartilage of the ulna and digit 4.
275 TAT-Cre bead placement (arrow) for the ulna in the Chameleon 17HH wing bud (**F**) and for
276 the ZPA in the Chameleon 18HH wing bud (**I**) with subsequent wholemounts in (**G**) and (**J**).
277 Sections show that fluorescent cells are within ulna cartilage for bead placed outside the ZPA
278 (**H**) but also for beads placed within the ZPA (**K**). Homotopic tdTom ZPA to eGFP grafts in
279 18HH wing buds (**L**) to confirm contribution of tdTom to a minority of ulna cartilage but also
280 to digit 3 cartilage shown in wholemount (**M**) and sections (**N**, **O**). TAT-Cre bead placement
281 in the ZPA of Chameleon 18HH hindlimb (**P**) with wholemount (**Q**) and sections (**R**, **S**)
282 showing ZPA lineage in the fibula and digit 4. Straight black and white lines denote the
283 anterior-most edge of somite 19. Abbreviations HH: Hamburger Hamilton. R: Radius. U:
284 Ulna. T: Tibia. F: Fibula. d1/2/3/4/5: digit 1/2/3/4/5. All scale bars = 200μm

285 Apical ectoderm ridge excision experiments of both Saunders (1948) and Summerbell (1974)
286 suggest that the proximal chicken ulna is specified before stage 20HH, so we therefore sought
287 to establish if the difference between mouse and chicken data could be resolved by
288 undertaking ZPA grafts earlier in development. We implanted TAT-Cre beads into the distal
289 limb mesenchyme of stage 18HH limbs at the axial level of anterior somite 19 (Fig. 4F) and
290 more posteriorly into the ZPA (Fig. 4I). Localisation of fluorescent clones were substantially
291 different between the experiments; beads placed in the "ulna region" at anterior somite 19
292 resulted in fluorescent labelling in the stylopod, the cartilage of the ulna and a small
293 contribution to the autopod (n=5/5; Fig. 4G, H). Beads placed in the ZPA, however, labelled
294 the stylopod, posterior limb mesenchyme of the zeugopod and autopod, but not the ulna
295 cartilage (n=4; Fig.4J, K). Additionally, we undertook homotopic grafting of dtTom ZPA
296 grafts to stage 18HH eGFP embryos (Fig. 4L). In this instance we did find that dtTom ZPA
297 grafts made a small contribution to posterior ulna and digit 3 (n=3/3; Fig. 4M-O), two of
298 which also contributed to the full length of the ulna. This work reconciles the origin of the
299 ulna between mouse and chicken, showing both have a small contribution of *SHH* expressing
300 cells along the posterior side of the ulna and digit 3 cartilages.

301 The chick hindlimb comprises of four digits and is considered to be a closer representative of
302 the pentadactyl limb of mice. The fourth digit of the chick leg is predominantly descended
303 from ZPA cells whilst the three anterior digits are not ZPA descendants, echoing ZPA
304 contributions to digits in mice (Towers, 2018). This suggests that there has been a loss of the
305 fifth digit in birds, which is reflective of fossil records of theropods. The zeugopod of the
306 chick hindlimb, fibula and tibia, are analogous to the ulna and radius of the forelimb,
307 respectively. To examine if the fibula, like the ulna of the mouse and chicken also arises
308 predominantly from *SHH*-/*PTCH1*+ cells, we implanted Tat-Cre beads into the ZPA of 18HH
309 hindlimb buds (Fig. 4P) and found surprisingly that the resulting fluorescent clones

310 contributed to the distal two-thirds of the fibula, the fourth metacarpal and phalanges of digit
311 4 (Fig. 4Q-S). This suggests a much larger contribution of SHH expressing cells form the
312 fibula than the ulna and demonstrates that even between the two posterior zeugopod bones of
313 birds (i.e. ulna and fibula), there is a considerable difference in the cellular lineages which
314 comprise them.

Discussion

Fate mapping approaches have been fundamental in developmental biology and the chicken embryo has been particularly useful in developing anatomical and temporal fate maps of developing tissues due to its anatomical accessibility. Limitations in technology, however, have also limited insights that can be made. Here we demonstrate a new anatomical approach to fate-mapping, which utilises topically applied TAT-Cre to a transgenic chicken containing a Cre-inducible transgene. This approach faithfully recreates and improves on fate maps of the chicken limb made by Saunders (1948), Vargesson et al (1997), Sato et al (2007) and others. With the creation of stably labelled genetic clones in anatomically discrete areas, we hope to be able to uncover the genetic and cellular regulatory networks that govern areas of the developing embryo which have been inaccessible to labelling by other means in chicken or mouse. Here, we used our approach to comment on a long-held conundrum in limb development; the evolution of the tridactyl limb and homologies in the developing limbs of mice and chickens.

The evolution of modern birds with powered flight from basal ground-based dinosaurs has captivated the interest of scientists for more than 200 years as a premier example of a major evolutionary transformation (Brusatte, 2017). Evidence from the fossil record indicates that the path to the evolution of powered flight was likely multifactorial and piecemeal, requiring many anatomical changes in the skeletal, musculature, respiratory and integument systems (Brusatte, 2017; Brusatte et al., 2014; Dececchi and Larsson, 2009; Xu et al., 2014). Few evolutionary trends towards powered flight, however, have been as commented on or contested as the dramatic reduction from the five fingered pentadactyl hand of the basal archosaurs to the tridactyl wing of modern birds, which have drawn evidence both from palaeontological and embryological perspectives in order to understand the mechanisms by which digits were lost (reviewed Xu and Mackem, 2013). Fate-mapping to establish the

origin of avian digits, as well as ascertaining the contribution of SHH signaling and *SHH* expressing cells to digits, has been used to support the evolutionary origin and therefore digit identity in modern birds, although interpretation can support both the frame-shift and axis-shift models (de Bakker et al., 2013; Kawahata et al., 2019; Tamura et al., 2011; Towers et al., 2011).

In the pentadactyl mouse limb, three main identifiers can be used to describe digit 4; articulation with the ulna as an extension of the primary axis, the first in order of appearance as a *Sox9*+ or alcian blue+ anlage over other digits (Shubin and Alberch, 1986) and derivation from *SHH* expressing cells (Harfe et al., 2004). These identifiers have also been applied to tridactyl bird wings to establish digit identity. As no digits in the chicken wing are derived from the *SHH* expressing lineage, it can be concluded that there has been a homeotic change in digit 4 identity to digit 3 via a possible change in SHH gradient (Tamura et al., 2011) or that digits 4 and 5 have been lost in the tridactyl wing evidenced by the lack of ZPA progeny found in the third digit (Towers et al., 2011), respectively. Furthermore, the tetradactyl chicken leg is concluded to have digits 1 through 4, as the fourth digit contains ZPA descendants (Towers et al., 2011).

Our finding that ZPA descendants contribute to the distal carpal 3 and posterior digit 3 metacarpal in the chicken is different from Towers et al 2011, but we believe it is due to the greater enhancement in visualisation of grafted cells through use of two transgenic reporter lines. This does not, however, change the interpretations of Towers et al (2011); digit 3 cartilage of the mouse also contains *SHH* expressing cells and by this measure we interpret that digit 3 in mouse and chicken are analogous. In summary, we find that the most posterior digit in the chicken wing is similar to digit 3 in the mouse, supporting the loss of digit 4 and 5 during evolution of the bird wing.

364 The zeugopod element of the primary axis, i.e. the ulna, is treated as a fixed and un-altered
365 point, from which digit number and articulation subsequently change. Indeed, compared to
366 digits, the ulna does superficially seem unaltered as it features in the majority of tetrapod
367 limbs, from stem tetrapods such as the acanthostega to modern vertebrates. There are only
368 two bones in the zeugopod; thus, its post-axial position and earlier condensation in relation to
369 the other bone, the radius, appear to satisfy the criteria for the ulna. This principle extends to
370 the hindlimb with the fibula recognised as analogous to the ulna (Towers, 2018). Due to the
371 apparent conservation of the zeugopod skeleton, the distribution of ZPA descendants to the
372 ulna of the pentadactyl limb in comparison to the tridactyl limb, or indeed to the fibula, has
373 not yet been investigated.

374 In both the mouse and chicken, the ulna is dependent on SHH signaling as shown by its
375 absence in *Shh* knockout mice (Chiang et al., 2001; Kraus et al., 2001) and OZD chicken, in
376 which limb-specific SHH signaling is lost (Ros et al., 2003). We mapped the chick ulna in the
377 stage HH20 limb bud, showing that it consistently arises from a highly discrete area that is
378 adjacent to anterior somite 19 and predominantly outside of the ZPA (Fig. 5A, B). Its stage
379 HH20 primordium is *SHH*- but *PTCH1*+, suggesting that the ulna is primarily patterned
380 through paracrine SHH activity. Overall, the mouse and chicken ulna both appear to be
381 largely subject to paracrine SHH signaling but have a varied distribution of *SHH* descendants.

382 In the OZD chicken, the fibula is also lost (Ros et al., 2003). However, unlike the ulna, we
383 found that the majority of fibular cartilage is derived from SHH expressing cells, suggesting
384 mostly autocrine SHH signaling. Digit identity as determined by ZPA contribution is often
385 used as a fixed preliminary for proposing hypotheses for limb variations across species but
386 also interchangeably between the fore and hind limbs. However, we show that even structures
387 considered to be fixed and conserved like the post-axial zeugopod bone cannot be unified via
388 the proportion of *SHH* expressing cells in its makeup.

This limitation has been acknowledged (Xu and Mackem, 2013) and through RNA sequencing of digits across five species, it has been shown that apart from digit 1, there is little homology in the expression profiles over digits 2 to 5 including that of *SHH* (Stewart et al., 2019). They conclude that the three digits of the avian wing correspond to the current amniotes expression profiles of digits 1, 3 and 4. RNA sequencing for the ulna and fibula are not yet completed but we do not expect such conservation of gene expression across species as demonstrated in digit 1 for the post-axial bone of the zeugopod. Instead, the differences in ZPA contributions between the mouse ulna, chick ulna and chick fibula indicate a composite nature of a singular anatomical structure, consisting of a complicated underlying developmental course and dynamic, piecemeal evolutionary change of its own.

Our results also suggest that the primary axis and ZPA lineage are not consistently related (Fig. 5C-F). The ulna and fibula are acknowledged to be a fixed element of the primary axis and digits have often been identified by their articulation and order of appearance in relation to the ulna or fibula (Larsson and Wagner, 2002; Shapiro et al., 2003). If there are variations in ZPA contributions between the ulna and fibula and also between species, perhaps the primary axis can also run through any digit regardless of its ZPA lineage, not just through digit 4 as has been the mainstay of digit identification. In mammals that demonstrate a reduction in SHH signaling and subsequently a loss of digits such as the pig and cow, the primary axis is maintained as with the mouse patterning, through the ulna articulating with digit 4 (Cooper et al., 2014; Tissieres et al., 2020). However, in birds with a delay and reduction in relative SHH signaling, which cause a loss of posterior digits and carpals such as the emu, the ulna articulation shifts anteriorly to digit 3 (Kawahata et al., 2019; Smith et al., 2016), suggesting digit identity as determined by SHH lineage does not dictate the course of the primary axis.

413 In conclusion, we show although the mouse and chicken ulna are predominantly *SHH*-,
414 suggesting paracrine patterning. Unlike the ulna, chick fibular cartilage is mostly descended
415 from the ZPA and thus, although the postaxial zeugopod is seen as fixed and often considered
416 as analogous, we demonstrate that these actually have different constituents of SHH lineage.
417 The ulna and fibula may be more evolutionarily diverse than supposed and therefore, their
418 participation in the primary axis may be flexible and unrelated to ZPA lineage. We suggest
419 that with changes in digit number, the articulation of the zeugopod with the autopod have
420 correspondingly developed to accommodate functionality over digit identity and that the
421 zeugopod will have adapted just as much as digits, alluded to by the variation in contributions
422 of *SHH* expressing cells.

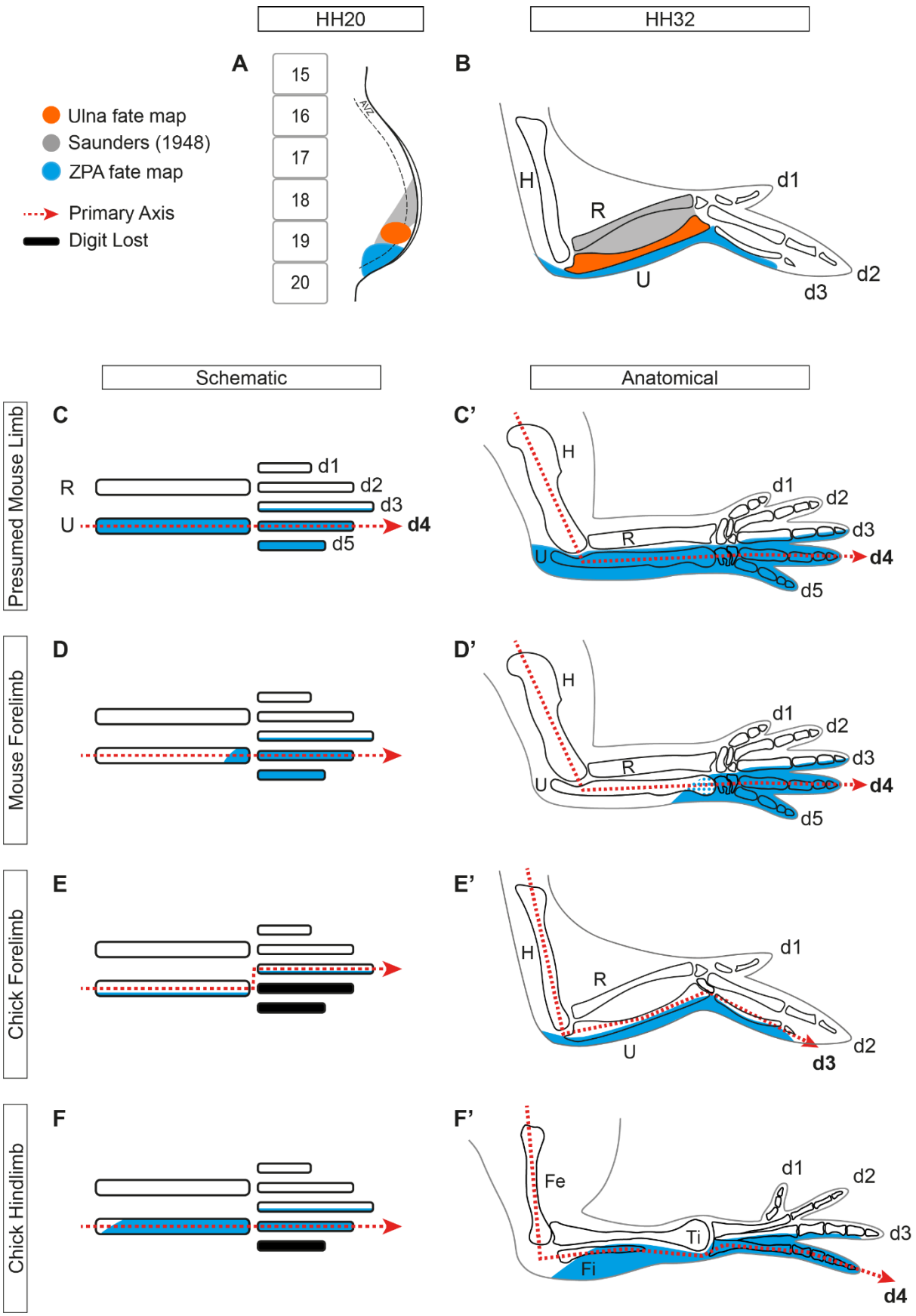
HH20
HH32
A
B
15
16
17
18
19
20
AVZ
Ulna fate map
Saunders (1948)
ZPA fate map
Primary Axis
Digit Lost
H
R
U
d1
d2
d3
Schematic
Anatomical
Presumed Mouse Limb
Mouse Forelimb
Chick Forelimb
Chick Hindlimb
C
C'
D
D'
E
E'
F
F'
d4
d5
Fe
Ti
Fi

423

Figure 5. Summary schematic of ulna fate map and ZPA lineage in relation to the primary axis

Updated fate map with the inclusion of our findings in orange (**A**, **B**). The ulna arises from the anterior half of somite 19 in the distal 20HH chick wing bud (**A**).

Schematic and anatomical representations of the mouse forelimb bones with the primary axis going through the ulna and digit 4 with the presumption that the ZPA contributes to the ulna, digit 4 and digit 5 (Krawchuk et al., 2010; Zhu et al., 2022) (**C**, **C'**). Current findings that only the distal ulna of the mouse forelimb is derived from ZPA cells, demonstrating that the primary axis and ZPA lineage are not congruent (**D**, **D'**). ZPA cells contribute to the posterior-most ulna but unlike the mouse, the entire length (**E**, **E'**). If the primary axis is maintained through digit 4, then the chick wing has had no shift, maintaining the divergence of ZPA lineage to the primary axis. The fibula and digit 4 of the chick hindlimb are derived from ZPA cells (**F**, **F'**), illustrating that the ZPA lineage of the posterior zeugopod bone is not conserved, even within species.

<u>Abbreviations</u> HH: Hamburger Hamilton. AVZ: Avascular zone. H: Humerus. R: Radius. U: Ulna. d1/2/3/4/5: digit 1/2/3/4/5.

440 **Materials and Methods**

441 ***Chicken Husbandry***

442 ISA Brown, Roslin Green (Cytoplasmic GFP), Flamingo (TdTomato) and Chameleon
443 (Cytbow) chicken lines were maintained under Home Office License at the Roslin Institute.
444 Fertilised chicken eggs were incubated at 38°C until the desired stage of embryonic
445 development (Hamburger and Hamilton, 1951).

446 ***Mouse Construction and Genotyping***

447 Mice used in this study were housed at the animal facilities at the University of Edinburgh,
448 with procedures performed under Personal and Project Home Office Licences. Male mice
449 carrying the SHHtm1(EGFP/cre)Cjt allele (Harfe et al., 2004) were mated to female mice
450 carrying a Cre reporter line (Luche et al., 2007). Cre expression leads to excision of a floxed
451 transcriptional Stop cassette and allows expression of the tdRFP in all descendant cells.
452 Embryos were collected at E14.5, genotyped by standard methods and fixed overnight in 4%
453 PFA.

454 ***Homotopic Grafts***

455 At the desired stage, host sites of Roslin Green or ISA Brown embryos were dissected and
456 discarded using a tungsten dissecting needle. Donor sites from Flamingo embryos were
457 dissected and moved into the host Roslin Green embryo via a p20 pipette containing DMEM.
458 The graft was manoeuvred into the host site and, when necessary, secured with a piece of
459 0.02mm oxidised nickel chrome wire. Care was taken to ensure ectoderm orientation was
460 maintained between donor and host. Embryos for wholemount analysis were culled and
461 dissected at around stage 33HH, fixed and cleared with CUBIC reagent 1 before being
462 imaged on a Zeiss Axiozoom V16 microscope. Embryos for HCR in situ hybridisation were

allowed to incubate for 3 hours after graft insertion, then culled and dissected in cold DEPC PBS before being fixed with 4% PFA at 4°C overnight.

Chameleon Cytbow Chicken Manipulations

Fertilised eggs were windowed, prepared for manipulation as per Tiecke and Tickle (2007) and staged (Hamburger and Hamilton, 1951). Once bead manipulations were complete, the window was sealed with tape and incubated at 38°C in a humidified and light-free environment until the desired Hamburger and Hamilton stage. Embryos were culled in accordance with Schedule 1 of the Animals (Scientific Procedures) Act 1986. Embryos were dissected in cold PBS in preparation for staining or in-situ hybridisation.

Hybridisation Chain Reaction In Situ Hybridisation

Whole-mount tissue was prepared for HCR by dissecting in cold DEPC PBS and fixing in 4% PFA overnight. After washing twice in PBT for 5min each, fixed tissue were dehydrated with a series of MeOH/PBST washes for 5min each on ice. Once dehydrated up to 100% MeOH, tissue were stored in -20°C until further use. Prior to performing HCR, tissues were rehydrated with a series of MeOH/PBST washes for 5min on ice up to 100% PBST. Tissues were treated with 10ug/mL proteinase K solution at room temperature for a length of time that was calculated at 15sec per stage (e.g. 5min for stage 20HH). These were post-fixed in 4% PFA at room temperature, then washed twice in PBST for 5min each, 50% PBST/50% 5XSSCT for 5min, then 5XSSCT for 5min, all on ice. We then performed HCR v3.0 using the protocol as described by Molecular Instruments (Choi et al., 2018). Split initiator probes (v3.0) for *PTCH1* (accession #NM_204960.2) and *SHH* (accession #NM_204821.1) were designed by Molecular Instruments, Inc.

486 ***Sections***

487 Embryos were dissected in cold PBS and fixed in 4% PFA overnight. After sucrose
488 treatment, limbs were embedded in a solution of 7.5% gelatin and 15% sucrose in PBS then
489 frozen in isopentane at around -60°C and stored at -80°C until sectioning. Serial sections
490 were obtained with a Bright OTF5000 cryostat microtome at a 10um thickness and mounted
491 on Polysine Adhesion microscope slides. Once dry, slides were washed in PBS at 37°C and
492 mounted with coverslips. Images were obtained on the LSM880 Confocal microscope using
493 Zen Black software.

494 ***Clearing***

495 Fixed tissues were washed in PBS for 5min at room temperature then submerged in CUBIC
496 reagent 1A (as per Susaki et al., 2015) at 37°C for 2-6 hours until cleared.

497 ***PCR***

498 Five samples of ulna and ZPA were dissected from 20HH ISA Brown embryos and batched
499 for a single reaction. These were stored at -80ºC before RNA extraction using Pre cellys bead
500 homogenisation (Bertin Technologies, France) and RNA easy Kit (Qiagen). Turbo DNA free
501 DNase kit (Ambion) was used to remove genomic DNA contamination before cDNA was
502 synthesised using AffinityScript Multiple Temperature cDNA Synthesis Kit (Agilent) using
503 Oligo DT. Triplicate qRT-PCR reactions were carried out per biological replicate using an
504 MX 3005P thermal cycler (Agilent) using a FAST 2 step thermal cycling protocol (95ºC 10
505 sec, 60ºC 30 sec). Brilliant iii Ultra Fast SYBR green qPCR master mix (Agilent) and
506 Chicken primers were used at 100nM final and were as follows: LBR F:
507 GAAGCTGCAGTACCGGATCA, LBR R: GCTAGGTCTTCCTCAGGTGC (housekeeping
508 gene). SHH (accession #NM_204821.1) F: CCAAATTACAACCCTGAC, SHH
509 R:CATTCAGCTTGTCCTTGCAG, PTCHD1 F: TGGGAAATACAATTCCACCTTC,

510 PTCHD1 R: CTCCAGGAGGACAACATTTCA. Data was analysed using MX Pro software
511 and exporting to Excel where a 2-ddCT method was used to calculate relative expression
512 compared to ZPA.

Contributions

Conceptualization: MGD and JDHO

Methodology and resources: MGD, JDHO, DDZS, LM, MJ, JG, JJS, LAL

Analysis and investigation: MGD, JDHO, MJ, JG

Writing – Original Draft: MGD and JDHO/All authors contributed to manuscript review and editing.

Acknowledgments

We thank the National Avian Research Facility, The Roslin Institute and R(D)SVS for the maintenance and production of fertile eggs from the Chameleon, dtTomato, GFP lines. This study was funded by Biotechnology and Biological Sciences Research Council (BBSRC) to The Roslin Institute, BB/X010937/1, BB/CCG2270/1 and to the Institute of Genetics and Cancer by the Medical Research Council (MRC) University Unit programmes MC_UU_00007/8 and MC_UU_00035/7. JDHO is supported by a University of Edinburgh Principals Studentship and The Roslin Institute.

Competing Interests

The authors state that they have no financial and non-financial competing interests.

Ethical Considerations

All animal experiments were reviewed and approved by the University of Edinburgh Animal Welfare and Ethics Committee and were conducted with appropriate licensing under Animals (Scientific Procedures) Act 1986. All experiments on chicken embryos were undertaken for day 14 of incubation.

'For the purpose of open access, the author has applied a CC BY public copyright licence to any Author Accepted Manuscript version arising from this submission'

536 **References**

537 **Ahn, S. and Joyner, A. L.** (2004). Dynamic changes in the response of cells to positive
538 hedgehog signaling during mouse limb patterning. *Cell* **118**, 505-516.

539 **Baldarelli, R. M., Smith, C. M., Finger, J. H., Hayamizu, T. F., McCright, I. J., Xu, J.,**
540 **Shaw, D. R., Beal, J. S., Blodgett, O., Campbell, J., et al.** (2021). The mouse Gene
541 Expression Database (GXD): 2021 update. *Nucleic Acids Res* **49**, D924-D931.

542 **Bednar, M. S., James, M. A. and Light, T. R.** (2009). Congenital longitudinal deficiency. *J*
543 *Hand Surg Am* **34**, 1739-1747.

544 **Botelho, J. F., Ossa-Fuentes, L., Soto-Acuna, S., Smith-Paredes, D., Nunez-Leon, D.,**
545 **Salinas-Saavedra, M., Ruiz-Flores, M. and Vargas, A. O.** (2014). New
546 Developmental Evidence Clarifies the Evolution of Wrist Bones in the Dinosaur-Bird
547 Transition. *Plos Biology* **12**, e1001957.

548 **Brusatte, S.** (2017). Taking wing. *Scientific American* **316**, 48-55.

549 **Brusatte, S. L., Lloyd, G. T., Wang, S. C. and Norell, M. A.** (2014). Gradual assembly of
550 avian body plan culminated in rapid rates of evolution across the dinosaur-bird
551 transition. *Curr Biol* **24**, 2386-2392.

552 **Burke, A. C. and Feduccia, A.** (1997). Developmental patterns and the identification of
553 homologies in the avian hand. *Science* **278**, 666-668.

554 **Chatterjee, S.** (1998). Counting the Fingers of Birds and Dinosaurs. *Science* **280**, 355-355.

555 **Chiang, C., Litingtung, Y., Harris, M. P., Simandl, B. K., Li, Y., Beachy, P. A. and**
556 **Fallon, J. F.** (2001). Manifestation of the limb prepattern: limb development in the
557 absence of sonic hedgehog function. *Dev Biol* **236**, 421-435.

558 **Choi, H. M. T., Schwarzkopf, M., Fornace, M. E., Acharya, A., Artavanis, G.,**
559 **Stegmaier, J., Cunha, A. and Pierce, N. A.** (2018). Third-generation in situ

560 hybridization chain reaction: multiplexed, quantitative, sensitive, versatile, robust.
561 *Development (Cambridge, England)* **145** (12).
562 **Cooper, K. L., Sears, K. E., Uygur, A., Maier, J., Baczkowski, K. S., Brosnahan, M.,**
563 **Antczak, D., Skidmore, J. A. and Tabin, C. J.** (2014). Patterning and post-
564 patterning modes of evolutionary digit loss in mammals. *Nature* **511**, 41-45.
565 **Davey, M. G., Balic, A., Rainger, J., Sang, H. M. and McGrew, M. J.** (2018). Illuminating
566 the chicken model through genetic modification. *Int J Dev Biol* **62**, 257-264.
567 **de Bakker, M. A., Fowler, D. A., den Oude, K., Dondorp, E. M., Navas, M. C.,**
568 **Horbanczuk, J. O., Sire, J. Y., Szczerbinska, D. and Richardson, M. K.** (2013).
569 Digit loss in archosaur evolution and the interplay between selection and constraints.
570 *Nature* **500**, 445-448.
571 **de Bakker, M. A. G., van der Vos, W., de Jager, K., Chung, W. Y., Fowler, D. A.,**
572 **Dondorp, E., Spiekman, S. N. F., Chew, K. Y., Xie, B., Jimenez, R., et al.** (2021).
573 Selection on Phalanx Development in the Evolution of the Bird Wing. *Mol Biol Evol*
574 **38**, 4222-4237.
575 **Dececchi, T. A. and Larsson, H. C.** (2009). Patristic evolutionary rates suggest a punctuated
576 pattern in forelimb evolution before and after the origin of birds. *Paleobiology* **35**, 1-
577 12.
578 **Dudley, A. T., Ros, M. A. and Tabin, C. J.** (2002). A re-examination of proximodistal
579 patterning during vertebrate limb development. *Nature* **418**, 539-544.
580 **Gros, J. and Tabin, C. J.** (2014). Vertebrate limb bud formation is initiated by localized
581 epithelial-to-mesenchymal transition. *Science* **343**, 1253-1256.
582 **Hamburger, V. and Hamilton, H. L.** (1951). A series of normal stages in the development
583 of the chick embryo. *Journal of Morphology* **88**, 49-92.

584 **Harfe, B. D., Scherz, P. J., Nissim, S., Tian, H., McMahon, A. P. and Tabin, C. J.** (2004).
585 Evidence for an expansion-based temporal Shh gradient in specifying vertebrate digit
586 identities. *Cell* **118**, 517-528.
587 **Hinchliffe, J. and Hecht, M.** (1984). Homology of the bird wing skeleton: embryological
588 versus paleontological evidence. In *Evolutionary Biology: Volume 18*, pp. 21-39:
589 Springer.
590 **Ianakiev, P., van Baren, M. J., Daly, M. J., Toledo, S. P. A., Cavalcanti, M. G., Neto, J.**
591 **C., Silveira, E. L., Freire-Maia, A., Heutink, P., Kilpatrick, M. W., et al.** (2001).
592 Acheiropodia is caused by a genomic deletion in C7orf2, the human orthologue of the
593 Lmbr1 gene. *American Journal of Human Genetics* **68**, 38-45.
594 **Kawahata, K., Cordeiro, I. R., Ueda, S., Sheng, G., Moriyama, Y., Nishimori, C., Yu, R.,**
595 **Koizumi, M., Okabe, M. and Tanaka, M.** (2019). Evolution of the avian digital
596 pattern. *Scientific Reports* **9(1): 8560**
597 **Kraus, P., Fraidenraich, D. and Loomis, C. A.** (2001). Some distal limb structures develop
598 in mice lacking Sonic hedgehog signaling. *Mechanisms of Development* **100**, 45-58.
599 **Krawchuk, D., Weiner, S. J., Chen, Y. T., Lu, B. C., Costantini, F., Behringer, R. R. and**
600 **Laufer, E.** (2010). Twist1 activity thresholds define multiple functions in limb
601 development. *Dev Biol* **347**, 133-146.
602 **Larsson, H. C. E. and Wagner, G. N. P.** (2002). Pentadactyl ground state of the avian wing.
603 *Journal of Experimental Zoology* **294**, 146-151.
604 **Luche, H., Weber, O., Nageswara Rao, T., Blum, C. and Fehling, H. J.** (2007). Faithful
605 activation of an extra-bright red fluorescent protein in "knock-in" Cre-reporter mice
606 ideally suited for lineage tracing studies. *European journal of immunology* **37**, 43-53.
607 **Mariani, F. V., Ahn, C. P. and Martin, G. R.** (2008). Genetic evidence that FGFs have an
608 instructive role in limb proximal-distal patterning. *Nature* **453**, 401-405.

609 **Markman, S., Zada, M., David, E., Giladi, A., Amit, I. and Zelzer, E.** (2023). A single-
610 cell census of mouse limb development identifies complex spatiotemporal dynamics
611 of skeleton formation. *Developmental cell* **58**, 565-581.
612 **McCusker, C. and Rosello-Diez, A.** (2022). In preprints: new insights into proximodistal
613 limb patterning and differentiation. *Development (Cambridge, England)* **149** (19).
614 **Nomura, N., Yokoyama, H. and Tamura, K.** (2014). Altered developmental events in the
615 anterior region of the chick forelimb give rise to avian-specific digit loss.
616 *Developmental dynamics : an official publication of the American Association of*
617 *Anatomists* **243**, 741-752.
618 **Richardson, M. K.** (2012). Manus horribilis: the chicken wing skeleton. In *From Clone to*
619 *Bone*, pp. 328-362. United Kingdom: Cambridge University Press.
620 **Richardson, M. K., Gobes, S. M., van Leeuwen, A. C., Polman, J. A., Pieau, C. and**
621 **Sanchez-Villagra, M. R.** (2009). Heterochrony in limb evolution: developmental
622 mechanisms and natural selection. *J Exp Zool B Mol Dev Evol* **312**, 639-664.
623 **Ros, M. A., Dahn, R. D., Fernandez-Teran, M., Rashka, K., Caruccio, N. C., Hasso, S.**
624 **M., Bitgood, J. J., Lancman, J. J. and Fallon, J. F.** (2003). The chick
625 oligozeugodactyly (ozd) mutant lacks sonic hedgehog function in the limb.
626 *Development (Cambridge, England)* **130**, 527-537.
627 **Rosello-Diez, A., Ros, M. A. and Torres, M.** (2011). Diffusible signals, not autonomous
628 mechanisms, determine the main proximodistal limb subdivision. *Science* **332**, 1086-
629 1088.
630 **Salinas-Saavedra, M., Gonzalez-Cabrera, C., Ossa-Fuentes, L., Botelho, J. F., Ruiz-**
631 **Flores, M. and Vargas, A. O.** (2014). New developmental evidence supports a
632 homeotic frameshift of digit identity in the evolution of the bird wing. *Front Zool* **11**,
633 33.

634 **Sato, K., Koizumi, Y., Takahashi, M., Kuroiwa, A. and Tamura, K.** (2007). Specification
635 of cell fate along the proximal-distal axis in the developing chick limb bud.
636 *Development (Cambridge, England)* **134**, 1397-1406.
637 **Saunders, J. W., Jr.** (1948). The proximo-distal sequence of origin of the parts of the chick
638 wing and the role of the ectoderm. *J Exp Zool* **108**, 363-403.
639 **Scherz, P. J., McGlinn, E., Nissim, S. and Tabin, C. J.** (2007). Extended exposure to Sonic
640 hedgehog is required for patterning the posterior digits of the vertebrate limb. *Dev*
641 *Biol* **308**, 343-354.
642 **Shapiro, M. D., Hanken, J. and Rosenthal, N.** (2003). Developmental basis of evolutionary
643 digit loss in the Australian lizardHemiergis. *Journal of Experimental Zoology* **297B**,
644 48-56.
645 **Shubin, N. H. and Alberch, P.** (1986). A Morphogenetic Approach to the Origin and Basic
646 Organization of the Tetrapod Limb. In *Evolutionary Biology: Volume 20* (ed. M. K.
647 Hecht, B. Wallace & G. T. Prance), pp. 319-387. Boston, MA: Springer US.
648 **Smith, C. A., Farlie, P. G., Davidson, N. M., Roeszler, K. N., Hirst, C., Oshlack, A. and**
649 **Lambert, D. M.** (2016). Limb patterning genes and heterochronic development of the
650 emu wing bud. *Evodevo* **7**, 26.
651 **Smithson, T. R., Carroll, R. L., Panchen, A. L. and Andrews, S. M.** (2011). Westlothiana
652 lizziaefrom the Viséan of East Kirkton, West Lothian, Scotland, and the amniote
653 stem. *Earth and Environmental Science Transactions of the Royal Society of*
654 *Edinburgh* **84**, 383-412.
655 **Stewart, T. A., Liang, C., Cotney, J. L., Noonan, J. P., Sanger, T. J. and Wagner, G. P.**
656 (2019). Evidence against tetrapod-wide digit identities and for a limited frame shift in
657 bird wings. *Nat Commun* **10**, 3244.

658 **Summerbell, D.** (1974). Interaction between the proximo-distal and antero-posterior co-
659 ordinates of positional value during the specification of positional information in the
660 early development of the chick limb-bud. *Development (Cambridge, England)* **32**,
661 227-237.
662 **Susaki, E. A., Tainaka, K., Perrin, D., Yukinaga, H., Kuno, A. and Ueda, H. R.** (2015).
663 Advanced CUBIC protocols for whole-brain and whole-body clearing and imaging.
664 *Nat Protoc* **10**, 1709-1727.
665 **Tamura, K., Nomura, N., Seki, R., Yonei-Tamura, S. and Yokoyama, H.** (2011).
666 Embryological evidence identifies wing digits in birds as digits 1, 2, and 3. *Science*
667 **331**, 753-757.
668 **Tickle, C.** (2015). How the embryo makes a limb: determination, polarity and identity. *J*
669 *Anat* **227**, 418-430.
670 **Tiecke, E. and Tickle, C.** (2007). Application of sonic hedgehog to the developing chick
671 limb. *Methods Mol Biol* **397**, 23-33.
672 **Tissieres, V., Geier, F., Kessler, B., Wolf, E., Zeller, R. and Lopez-Rios, J.** (2020). Gene
673 Regulatory and Expression Differences between Mouse and Pig Limb Buds Provide
674 Insights into the Evolutionary Emergence of Artiodactyl Traits. *Cell Rep* **31**, 107490.
675 **Towers, M.** (2018). Evolution of antero-posterior patterning of the limb: Insights from the
676 chick. *Genesis* **56**, e23047.
677 **Towers, M., Mahood, R., Yin, Y. and Tickle, C.** (2008). Integration of growth and
678 specification in chick wing digit-patterning. *Nature* **452**, 882-886.
679 **Towers, M., Signolet, J., Sherman, A., Sang, H. and Tickle, C.** (2011). Insights into bird
680 wing evolution and digit specification from polarizing region fate maps. *Nat Commun*
681 **2**, 426.

682 **Towers, M. and Tickle, C.** (2009). Growing models of vertebrate limb development.
683 *Development (Cambridge, England)* **136**, 179-190.
684 **Vargas, A. O. and Fallon, J. F.** (2005). The digits of the wing of birds are 1, 2, and 3. A
685 review. *J Exp Zool B Mol Dev Evol* **304**, 206-219.
686 **Vargesson, N., Clarke, J. D., Vincent, K., Coles, C., Wolpert, L. and Tickle, C.** (1997).
687 Cell fate in the chick limb bud and relationship to gene expression. *Development*
688 *(Cambridge, England)* **124**, 1909-1918.
689 **Welten, M. C., Verbeek, F. J., Meijer, A. H. and Richardson, M. K.** (2005). Gene
690 expression and digit homology in the chicken embryo wing. *Evol Dev* **7**, 18-28.
691 **Woltering, J. M. and Duboule, D.** (2010). The origin of digits: expression patterns versus
692 regulatory mechanisms. *Developmental cell* **18**, 526-532.
693 **Xu, X. and Mackem, S.** (2013). Tracing the evolution of avian wing digits. *Curr Biol* **23**,
694 R538-544.
695 **Xu, X., Zhou, Z., Dudley, R., Mackem, S., Chuong, C.-M., Erickson, G. M. and**
696 **Varricchio, D. J.** (2014). An integrative approach to understanding bird origins.
697 *Science* **346**, 1253293.
698 **Zhu, J., Patel, R., Trofka, A., Harfe, B. D. and Mackem, S.** (2022). Sonic hedgehog is not
699 a limb morphogen but acts as a trigger to specify all digits in mice. *Developmental*
700 *cell* **57**, 2048-2062 e2044.

701